An Operative Porphyry Copper Model Based on Thermochemical Evidence of Convective Gaseous Hydrogen Transport and Mega-Stratovolcanic Eruptions Containing Anhydrite

George Brimhall
Clementine Exploration LLC
Wise River MT and Berkeley CA
brimhall@clementinemt.com

Abstract

What do giant porphyry copper deposits and cataclysmic mega-strata volcano eruptions like Mount Pinatubo in the Philippines have in common besides the mineral anhydrite ($CaSO_4$)? Why do mineralized porphyry magmas explosively hydro-fracture and drive long-lived hydrothermal convection cells in the subsurface while some rare arc magmas instead erupt explosively to form stratovolcanoes with atmospheric impacts? These questions are answered here by invoking hydrogen gas H_2 rather than oxygen O_2 to gauge redox processes leading to anhydrite ($CaSO_4$) stability over that of titanite ($CaTiSiO_5$). The H_2 geochemical reference frame affords an opportunity to re-evaluate oxidation processes from first principles, free of assumptions and precedence. A thermodynamic diagram is developed here for redox equilibria in porphyry copper genesis using H_2 gas instead of O_2 which is not present. The H_2 vs 1/T Van't Hoff reference frame at water saturation works as a powerful operative geochemical diagram because confined-flow migration of H_2 by protracted magmatic outgassing during thermal advection causes oxidation by dehydrogenation and reduction in the return flow heating path approaching the pluton. Expulsion of highly oxidized early high temperature aqueous fluids continue to lose H_2 and oxidize along a cooling path defined by the Mg-rich (X_{Fe}=0.2), Ti-poor hydrothermal biotite-magnetite-K-feldspar Potassic alteration mineral assemblage line which serves as definitive trajectory of the cooling pathway. The return heating pathway is marked by Propylitic alteration and finally distal diffusion-controlled orbicular actinolite alteration. Two distinct concentric advective circulation cells emerge in the log H_2 vs. 1/T space. The largest advective circulation cell defines sediment-hosted Bingham-type PCD systems which reach both extreme early oxidative states with chalcopyrite, bornite and digenite (chalcocite) and extreme reductive states with distal actinolite orbicular alteration. In contrast, the batholith-hosted Butte-type PCD cell has a narrow limited early oxidation range which does not extend up to bornite or digenite and instead consists of only of chalcopyrite-pyrite. It also lacks a distal orb ring due to restrictive chemical buffering by the influence of granite wall rocks with red-colored high-Ti (X_{Fe}=0.5) biotite terminating in the advanced argillic assemblage with covellite and chalcocite on the oxidized end. Occurrences of actinolite orbs at Bingham, Escondida, El Hueso, Cajamarca, Morenci, Fortitude, Cananea, and Oyu Tolgoi imply that an actinolite orb ring may be a definitive indicator of large PCD systems. Given the necessity of electron conservation, a large actinolite orb ring portends a large highly-oxidized Potassic alteration zone with chalcopyrite, bornite and digenite. This potential exploration target size indicator supported by H_2 dynamics and redox thermochemistry may help guide discovery of new deep confined PCDs of considerable size and is being tested at the Clementine prospect in southwest Montana which has a 3 by 5 km orb ring. Besides realization that H_2 gas plays an important role in magma genesis

and ore deposition raises the possibility that it also has a chemo-mechanical impact of H_2 through hydrolytic weakening or embrittlement of silicate rock-forming minerals. If such weakening occurs the assumed stresses required for over-pressured fluids exsolved from magmas to induce brittle failure and promote explosive hydrofracturing could be dramatically reduced. Similarly, if hydrofracturing in the rigid carapace above volcanic magma chambers was induced at lower stress levels because of H_2-driven hydrolytic weakening, less energy is then required to drive the cataclysmic eruptions of super strata volcanoes. Porphyry copper deposits have been described as “failed” large volcanic eruptions. Conversely, oxidized anhydrite-bearing mega-strata volcanic eruptions containing anhydrite can be considered as once-potential porphyry copper magmas which upon exsolution of magmatic water breached the surface explosively rather than become a confined mineralized convective system at depth. Confinement in the case of porphyries, precludes the escape of H_2 to the atmosphere and instead promotes the downward advective transport of H_2 thus contributing to the formation of an upright barrel-shaped elliptical torus convective system centered on the cooling parental porphyry. Unlike stratovolcanoes, this deep reduced hydrothermal root system is conserved in porphyries when not destroyed by violent eruption. Speculatively, the dimensions in plan-view of the reduced actinolite orb ring may be forced by H_2 mass balance and electro-chemistry integrated over the scale of convection to be at least roughly proportional to the size of the coaxial central zone of oxidized copper sulfide formation. Hence, a potential exploration target size indicator supported by thermochemistry emerges from this use of the hydrogen geochemical perspective.

Introduction

In memory of Jim F. Luhr whose legacy to volcanology, like his music,
was made with rare insight, universal kindness, and joy.

While critical minerals and copper are vital to attaining a carbon neutral society through electrification, decarbonization of heavy industries, transportation, and aviation systems may require molecular hydrogen which is a powerful, portable, emission-free combustible fuel with a higher energy density (35 watts/g) than lithium (0.2 watts/g). However, the minute molecular size of H_2 (0.27 nm) makes it readily subject to diffusion even through many, but not all, metals and rocks making conveyance, storage, and petrological interpretation challenging. Such remarkably selective physical behavior raises the question as to where in nature hydrogen transport may have played an as yet unrecognized role of considerable importance. Especially for an abundant element in gaseous form hydrogen’s capability of affecting oxidation and reduction through its migration and electron transfer could have had major consequences on natural systems and so far has gone largely unrecognized although speculations infer that oxidation follows hydrogen escape by magmatic outgassing from volcanos to explain the higher oxidation state of arc magmas compared to other mantle-derived magma types. This assertion remains to date however a vague hypothesis and its resolution motivates this study to discover an operational mechanism.

There is a remarkable lack of high-temperature phase equilibria with which to start assessing the roles of H_2 in nature and quantitatively address H_2 outgassing. The paucity of relevant studies involving H_2 is likely due to the historical use of oxygen (O_2) in gauging redox states in nature rather than H_2. Therefore, to advance understanding of H_2 geochemistry beyond inference,

chemical thermodynamics is used here to construct new equilibrium phase diagrams where hydrogen is the principal variable of interest. Well-known recurrent Potassic and Propylitic mineral assemblages in PCD ore deposits of (Meyer and Hemley, 1967; Hemley and others, 1980; Lowell and Guilbert, 1970; Gustafson and Hunt, 1975; Sillitoe, 2010, and Johns et al, 2010) can then serve as recognizable markers defining both the cooling and heating pathways of convective fluid flow. For each mineral assemblage selected by the present author, the stoichiometry of each reaction has been computed defining the reaction coefficient mole numbers for each reactant and product. Once the reaction stoichiometry has been determined, equilibrium thermodynamic calculations have been made using the CHNOSZ thermodynamic code of Dick, 2019) to yield the equilibrium constants.

Although hydrogen may have escaped these geological systems en masse, in its wake is left a discernible mineralogical architecture in rocks that reveals the role of hydrogen over a wide temperature range from magmatic to hydrothermal conditions. One anhydrite-bearing mineral assemblage that is known to form under highly oxidizing conditions is common to both porphyry copper deposits (PCDs) and certain very large stratovolcanoes including El Chichon, Mexico where their similarities to PCDs has been noted (Luhr, 2008) including their occurrence with the tectonic metallogenic belt for PCDs known as the Ring of Fire located along a convergent tectonic plate boundary subduction zone. While their similarities are compelling including their water and sulfur-rich composition and high oxidation state, one telling difference is that while anhydrite has been shown to be a primary igneous mineral that formed from the crystallizing magma erupted to form volcanic ash, in porphyries in contrast, anhydrite precipitates from early high-temperature hydrothermal solutions. Given these similarities and differences, it is possible then that mega-strata volcanic eruptions with primary igneous anhydrite represent the sudden interruption of porphyry copper deposit development. Rather than develop a subsurface mineralized hydrothermal convective cell driven by the heat dissipation of the cooling porphyritic magma, the evolving magma body and the rigid carapace above the magma chamber failed, exploded, and erupted violently onto the earth’s surface and into the stratosphere. This study then explores what role hydrogen gas may have played in both cases; one hidden from human view in space and time- the other in contrast, leaving a vivid, lived memory of a globally cataclysmic event on the earth’s surface. This comparison of an intact subsurface ore deposit potentially contributing vital metals to a technologically-greener future versus its dissipation in a giant stratovolcano may provide a useful imagery for advancing public understanding of the immense physical scale of ore genesis and the unprecedented societal choices at stake. Social understanding of mineral resources and the necessity of mining in general is necessary now when critical and essential minerals including copper must be discovered to meet the accelerating industrial demands of decarbonization. Only though broad acceptance of this need based in some level of scientific understanding will a social license for mining be earned- at least within the United States.

Potential Impact of This Work

Explaining the origin and characteristics of a porphyry copper deposit is difficult at best even to professional geologists who are not specialists in mining geology or geochemistry. While a lay person may know about the Ring of Fire, volcanos and earthquakes related to subduction zones at convergent tectonic plate margins, few have any reference frame for appreciating a description

of porphyry ore deposits in terms of their size, crustal depth, multi-stage processes involving both magmas and aqueous fluids, the enormous energy involved, and singular importance as mineral resources of copper and a host of related chemical elements including sulfur. Without a meaningful reference frame, conveying the origin and importance of porphyry systems to the public can seem impossible. Furthermore most outcropping PCDs have already been discovered and are being mined, the genetic paradigm is out of date. The pre-mine surface of known PCDs intersected the cylindrical ore-forming column somewhere near its high-sulfide mid-section. Today, these outcropping systems are exceedingly rare and what is left are exposures of the low sulfide tops of much deeper PCDs which may well have an atypical surficial presentation lacking abundant stockworks and a leached capping. In fact, much less is known about the upper reaches of deep PCD systems requiring that a major revision be made of the prevailing exploration model (Brimhall, 2018; Brimhall and Fanning, 2019, and Brimhall 2021. The aspects of a new PCD exploration model that could be most impactful are those that can be recognized during early-stage exploration when a potentially large system could help motivate funding for deep drilling- an imperative that has long been recognized in Montana (Worthington, 2007). Since the zoning patterns of PCDs are concentric, the outermost shells then are likely to be encountered first. Therefore, correct interpretations of these outer hydrothermal rings could be disproportionally important.

Context

The thermochemical research described here involving hydrogen stems from on-going field-based studies and copper exploration in southwest Montana. First, advancement of the porphyry copper paradigm used in exploration based on detailed geological mapping at the Clementine prospect (Brimhall, 2018 and 2021) showed that distal actinolite (Fe-Tremolite) alteration with orbicules 1 to 2 cm in diameter forms a ring that surrounds the central vein gossan system and has also been noted at Bingham Canyon Utah where it was first recognized (Atkinson and Einaudi, 1978) in drill core. Actinolite orbs have also been noted at seven additional major porphyry copper deposits world-wide including Escondida, Morenci, and Oyu Tolgoi (Marco Einaudi- Personal Communication). Hence, a key objective here is to determine if an actinolite orb ring which formed by radial diffusive processes might surround only large, well-mineralized porphyries and hence provide a useful indicator of highly-prospective systems in contrast to smaller less economic occurrences.

How the Presence of H_2 Gas in Porphyries Was Recognized

In the process of advancing the porphyry copper model to include sedimentary wall rock interactions, Brimhall (2021) developed an isothermal-isobaric phase diagram using log fCO_2 /CH_4 vs log fH_2S coordinates presented **in Figure 1** computed for 300 degrees C and 500 bars (50 MPa). Along the right-hand side the redox state is shown using the conventional variable log fO_2 computed from the equilibria: $CH_4 + 2O_2 = CO_2 + 2H_2O$ and setting the value of the activity of H_2O at 1.0. In the process of seeking a still more realistic measure of redox state than log fO_2 which has miniscule values, log fH_2 values were computed from the equilibria: $2H_2O = 2H_2 + O_2$. These values are labeled in red just left of the log fO_2 values and are indeed much higher than are the log fO_2 values. Notice also that near the bottom of Figure 1 where the log fH_2 values are 0 to +1, that a number of reduced organic gases also occur including CH_4, n-Decane, n-

Hexane and Kerogen. Just above these organic gases orbicular actinolite alteration at both Bingham and Clementine occur along the outer edge of the actinolite stability field shown in green with co-exiting titanite and either magnetite or ilmenite within the biotite stability field shown in purple. Graphite becomes stable at logfH_2 just below the values where the orbicular alteration plots.

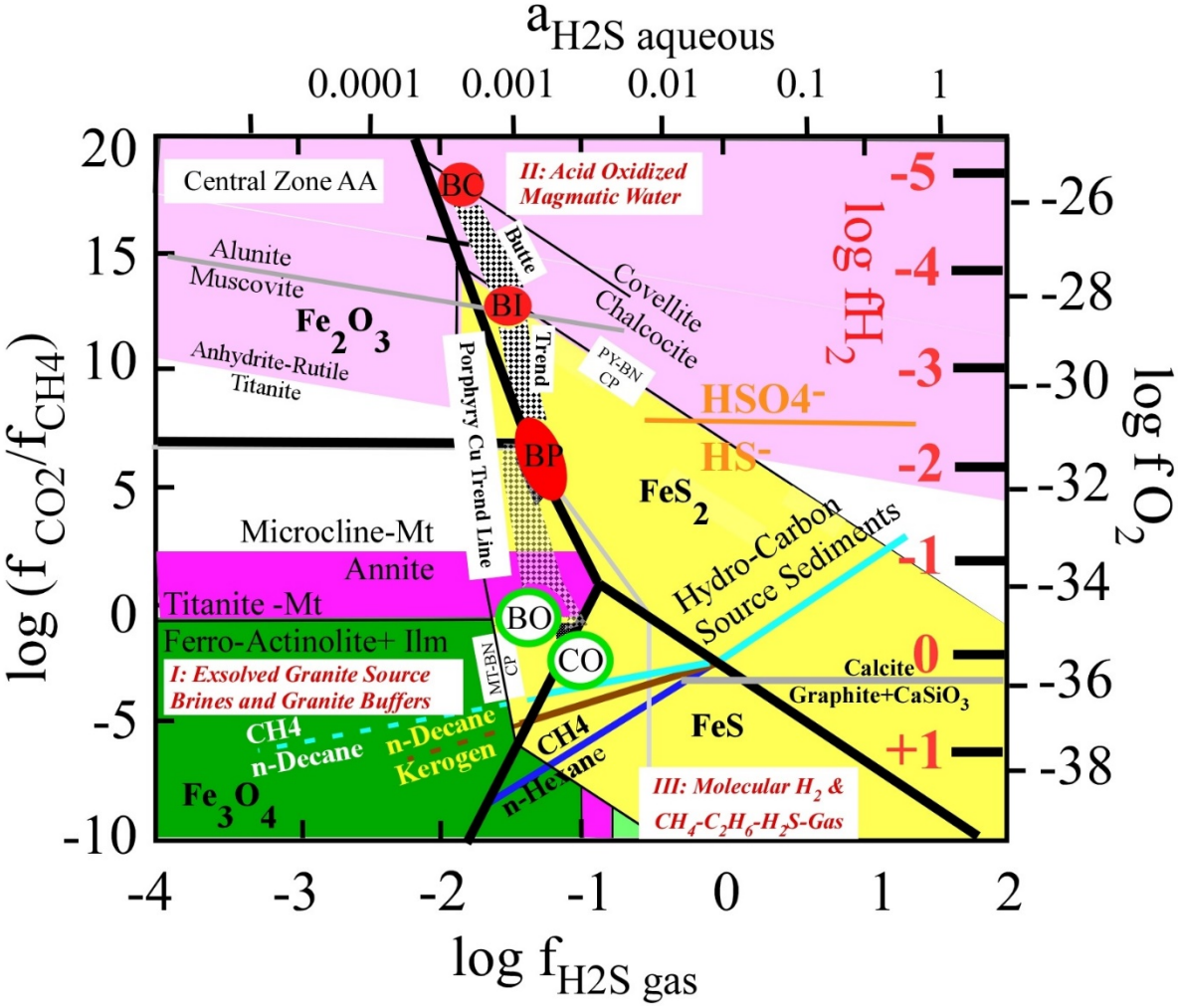

Figure 1. Isobaric (500 bars, 50 MPa) isothermal plot. On the right-hand vertical axis is logfO_2 is shown in black and corresponding logfH_2 in red which are far higher values signifying the actual presence of H_2 gas. Color patterns are as follows: dark green represents actinolite (Fe-Tremolite), purple represents biotite. Near the top of the figure are oxidizing conditions while the bottom reflect reducing condition. Pink represents anhydrite. Hydrocarbon source sediments are represented by a brown line (Kerogen/n-Decane), light blue line methane/n-Decane, and dark blue represents methane/n-Hexane equilibria. Porphyry copper deposits shown in stipples define a nearly vertical band in which the Butte pre-Main Stage (BP), Intermediate Zone (BI), and Central Zone (BC) with covellite-chalcocite and advanced argillic alteration (AA) and alunite occur forming the Butte Trend Line shown as a diamond checkerboard pattern. Orbicular actinolite alteration at the Bingham porphyry copper Mine in Utah (BO) and the Clementine

Prospect in Montana (CO) are shown as circles with a green rim and fall on the stippled porphyry Copper Trend Line.

Source of the Hydrogen

Unlike oxygen gas which was absent, hydrogen in contrast was present as a gas phase with a minute molecular size 0.27 nm making its diffusion through some of the most permeable surrounding rocks highly likely. A question as to the source of the hydrogen then arises. Two possibilities exist. First, hydrogen may have been derived locally from organics in the surrounding sedimentary wall rock sequence implied by the stability of methane, kerogen, n-Decane, and n-Hexan shown in **Figure 1**. However, the fact that the matrix rock between orbicular actinolite orbs has disseminated chalcopyrite, pyrrhotite, and ilmenite which are absent outside the orb ring implies that the source of H_2 was from fluids related somehow to the center of the district alteration zonation, vein gossan system, and plutons (Brimhall 2018, 2019, and 2021). The source of the fluid in the orbs is in fact proven to be from inside the orb ring and emanating from the center of the district by three facts: (1) the U/Pb SHRIMP date on titanite in the orbs of 70.7+/- 1.3 Million years is within analytical uncertainty of the age of a small altered pluton with titanite age of 72.7 +/- 1 Ma (Brimhall and Fanning, 2019). (2) multi-element geochemistry shows that the enrichment factor hierarchy of **Te> Se> Bi> As> Sb> Ag> Mo> W> Cu> pb> Zn** is the same for the orbs as it is for the vein gossans located at the center of the district positioned at the apex of a doubly-plunging anticline (**Figure 2**). Finally, orbicular alteration post-dates and alters all the lithologies shown in **Figure 2** proving that orb alteration is epigenetic.

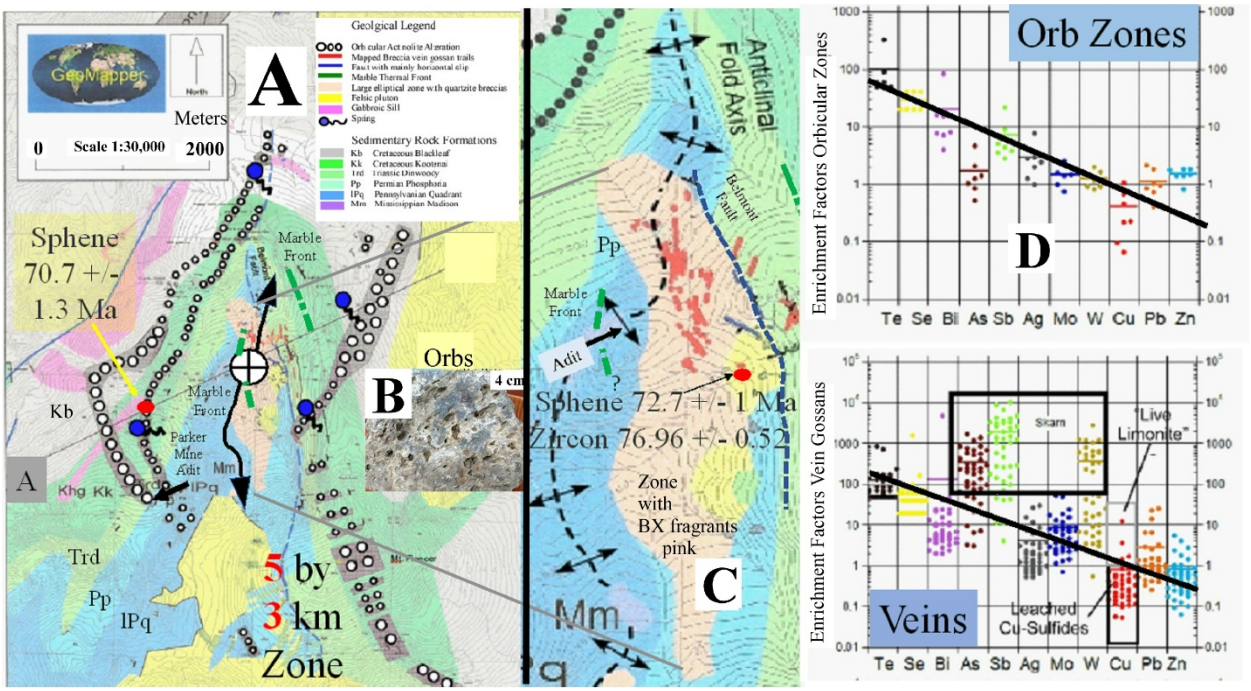

Figure 2. **A**. Geological map of the Clementine prospect in southwest Montana located between the southwest edge of the Boulder Batholith shown in yellow and the most northerly pluton of the Pioneer Mountains, the Big Hole River pluton, also in yellow. Springs are shown as black dots with squiggly black talk and occur within or near orb zones. **B**. Photograph of orbicular actinolite alteration shown in A with a stippled pattern. Rock between the orbs have disseminated chalcopyrite, pyrrhotite, and ilmenite. **C**. Enlargement of the map shown in **A** centered on the large elliptical zone containing barren quartz-rich breccias shown in pink which is 2.2 km-long. This breccia zone is centered on a doubly-plunging anticline co-axial with the surrounding actinolite orbicular rings and central zone containing a breccia vein gossan trail system shown in red with two small plutons in yellow just east of horizontal bedding symbol. The marble front is shown in a thick green line on the east side of the anticline and a green line on the west side where it has been approximately located. It is important to note that the orbicular actinolite bands occur outside of the marble front implying a lower temperature yet actinolite growth is related to the early high-temperature Potassic alteration expected at the deposit interior. SHRIMP dates on titanite in the orbs are shown. **D**. Enrichment Factors for the vein gossan systems below the Enrichment Factors for the actinolite orbs. Notice that both have the same hierarchy of from Te>Se>Bi>As>Sb>Ag>Mo>W>Cu>Pb>Zn. Veins closest to outcropping limestones show the effect of skarns enriched in As, Sb, and W with individual assays reaching over 2000 thousand ppm. Cu is leached but in samples with hematic limonite instead of goethite, Cu assays reach 800 ppm. All chemical analyses have been done by ALS Global in Sparks, Nevada using a four-acid rock pulp digestion and ICP-MS analysis for all elements. Crustal abundances used in computing the enrichment factors are from pTable.com

Retrospective Study of Ore-forming Mineral Assemblages

Rocks in ore deposits are among the most mineralogically complex rocks known on earth. Ores are formed by heat and mass transport processes which, while being part of the array of normal earth processes operative at vastly different scales from plate tectonics down to submicroscopic fluid inclusions, reach extreme enrichment levels rarely attained in nature (Brimhall, 1987). Today then, we study ores formed millions of years ago ex post facto. The causative hydrothermal fluids are now long-gone except for microscopic fluid inclusions in quartz and other minerals. Were gases present, they too are largely gone except for their occasional presence in fluid inclusions. If hydrogen is trapped within fluid inclusions, it may have at least partially diffused through minerals selectively and even diffused out of the fluid inclusions altogether. All post facto interpretations made today of the geochemistry of ore-forming fluids and gases are based on observations at different scales including mapped field relationships, observed mineral assemblages and sequences, structures including veins, veinlets, alteration envelopes, alteration zonation, miarolitic cavities, and fluid inclusion studies. Once the mineral assemblages and their temporal and spatial sequence are known and the physical conditions determined by geo-thermometry and geobarometry, then chemical thermodynamic calculations provide equilibrium phase diagrams in a coordinate space where each mineral assemblage can be located and used as a signpost to constrain and ultimately reconstruct the geochemical paths taken in nature. Theoretical fluid mechanics provides a second powerful tool to validate conclusions.

Methods for Computing Chemical Phase Equilibria and Thermodynamic Data Bases

A wealth of interdisciplinary knowledge supports the current understanding of porphyry copper deposit genesis and the mineral-solution equilibria involved. A variety of methods have been employed including hydrothermal experiment, hydro-fluoric acid solution calorimetry, and heat capacity measurements. Studies span biotite (Eugster and Wones, 1962 and 1965), alkali feldspar (Meyer and Hemley, 1967; Thompson and Waldbaum, 1967 and 1968) and magnetite (Eugster and Chou, 1977 and 1979). This work heralded the birth of experimental geochemistry at The Johns Hopkins, UC Berkeley, Harvard, Princeton, and Penn State among other universities as well as the Geophysical Lab of the Carnegie Institute, the Geochemistry and Petrology Branch of the USGS, and the US Bureau of Mines program on theoretical metallurgy (Kelly, 1960). Emerging from this voluminous research was an internally-consistent thermodynamic data base of Gibbs Free energy, Enthalpy, Volume, Entropy, and Heat Capacity functions summarized by the Helgeson Group at UC Berkeley in **SUPCRT92** Johnson et al, 1992 and made accessible for on-line computing using program **CHNOSZ** (Dick, 2019) which runs on the "**R**" on-line platform open to all users free of charge. Theoretical thermodynamic calculations herin are made possible by this complex internally consistent database and extensive use of **CHNOSZ**.

log fO_2 versus log fS_2 Diagrams

Among the first thermodynamic calculations of mineral-solution equilibria, Holland (1959), Meyer and Hemley (1967), Einaudi (1977), Brimhall (1980), and many others devised plots of log fO_2 versus log fS_2 to help explain reaction paths of ore forming solutions defined by sulfide, oxide, and silicate mineral assemblages and sequences. Hydrogen gas as such was not explored in these studies. Although experiments by Eugster and Wones used nested gold capsules to avoid hydrogen embrittlement of their steel pressure vessels which surrounded inner capsules of platinum to control fO_2 in experiments on granite mineral-solution equilibria, H_2 was considered as a challenging experimental factor to be controlled in order to define O_2 fugacity rather than as a prime geological variable of interest as it has become in this study.

Oxidation-Reduction Reactions involving H_2 Gas

Two different methods are discussed below that address the phase equilibria of H_2 gas and its geochemistry differently; one method lumps H_2 and H_2O together as a combined function so that they are inseparable, and the second method focusses on H_2 by itself by assuming that the aH_2O was unity.

Hydrogen Ratio R_H

Giggenbach (1987) proposed a redox variable called $R_H = \log (f H_2/f H_2O)$ as an alternative expression to log fO_2 asserting that it offered an estimate of the abundance of an actual reaction participant as the fugacities of O_2 in contrast are so low that they indicate essential no presence of oxygen gas as such. This inciteful approach was summarized later by Hedenquist in Einaudi and others, (2003). R_H does have the advantage of not having to know the activity or fugacity of H_2O to address H_2 indirectly, but this approach leaves open the question as to the actual value of H_2 fugacity which is the objective in this work. In the limit when the activity of H_2O equals a value of 1, then $R_H = \log f H_2$ otherwise R_H is a unitless ratio which in some ways is hard to interpret. To the extent that solutes lower the activity of H_2O in solution, R_H may over-estimate

the actual log fH_2. Hence, a different approach is taken here that develops an explicit value of log fH_2 consistent with the fact that hydrothermal solutions are intrinsically aqueous.

RESULTS

Here, rather than use the R_H which is rigorous but makes it difficult to separate and extract values of fH_2, it was decided to directly calculate fH_2 by assuming that the aH_2O was one. While the results are approximate, they may well be sufficiently accurate to form new useful conclusions.

Direct Discernment of Convective Cooling and Heating Paths

Interpreting complex multi-stage processes demands selection of a definitive analytical coordinate space which faithfully divulges nature's rules. **Figure 3 A** through **F** presents the systematic development of a new phase diagram in which log fH_2 is the variable of interest rather than fO_2. The vertical axis is log fH_2 and the horizontal axis is 1/T K absolute temperature relative to absolute zero with corresponding temperature in degrees Centigrade shown across the top of the diagram. Such a modified Van't Hoff plot showing log fH_2 rather than log K has several powerful advantages useful in geological interpretations. First, in Van't Hoff coordinates many equilibria plot as relatively straight lines with slopes proportional to the value of enthalpy of the reaction and the Y-intercept is proportional to entropy (Lewis and Randal, 1961). Second, depending upon the direction of temperature change, some lines represent cooling paths as hot magma-derived fluids undergo cooling towards the left. Similarly, other mineral-solution equilibria represent convective heating paths as temperature increases towards the right approaching a pluton. Assembly of this collection of lines which are vectors pointing either to the left for cooling or to the right for heating, identifies mineral assemblages in terms of their fluid flow direction. This graphical interpretation in a Van't Hoff plot yields cooling and heating paths directly and thus offers a viable straight forward alternative to far more complex calculations involved in parametric numerical modeling. Earlier work using Van't Hoff coordinates by Hedenquist in (Einaudi et al, 2003) was focused on defining the evolutionary pathways of multistage ore deposits and redox state of magmas especially demonstrating the continuity of fumaroles and magmatic-hydrothermal fluids using R_H calculated using Program QUILF (Andersen and others, 1993) in relation to geothermal fluids in shallow systems. In contrast, the use of Van't Hoff plots here is fundamentally different. Here, specific recurrent hydrothermal alteration and mineralization mineral assemblages including well-known variable biotite solid solution compositions are studied to ascertain the architecture of deeper convective magmatic-hydrothermal regimes and the role of wall rock buffering. In particular, proximal up-flow heating paths and distal down-flow cooling and finally heating return paths are revealed.

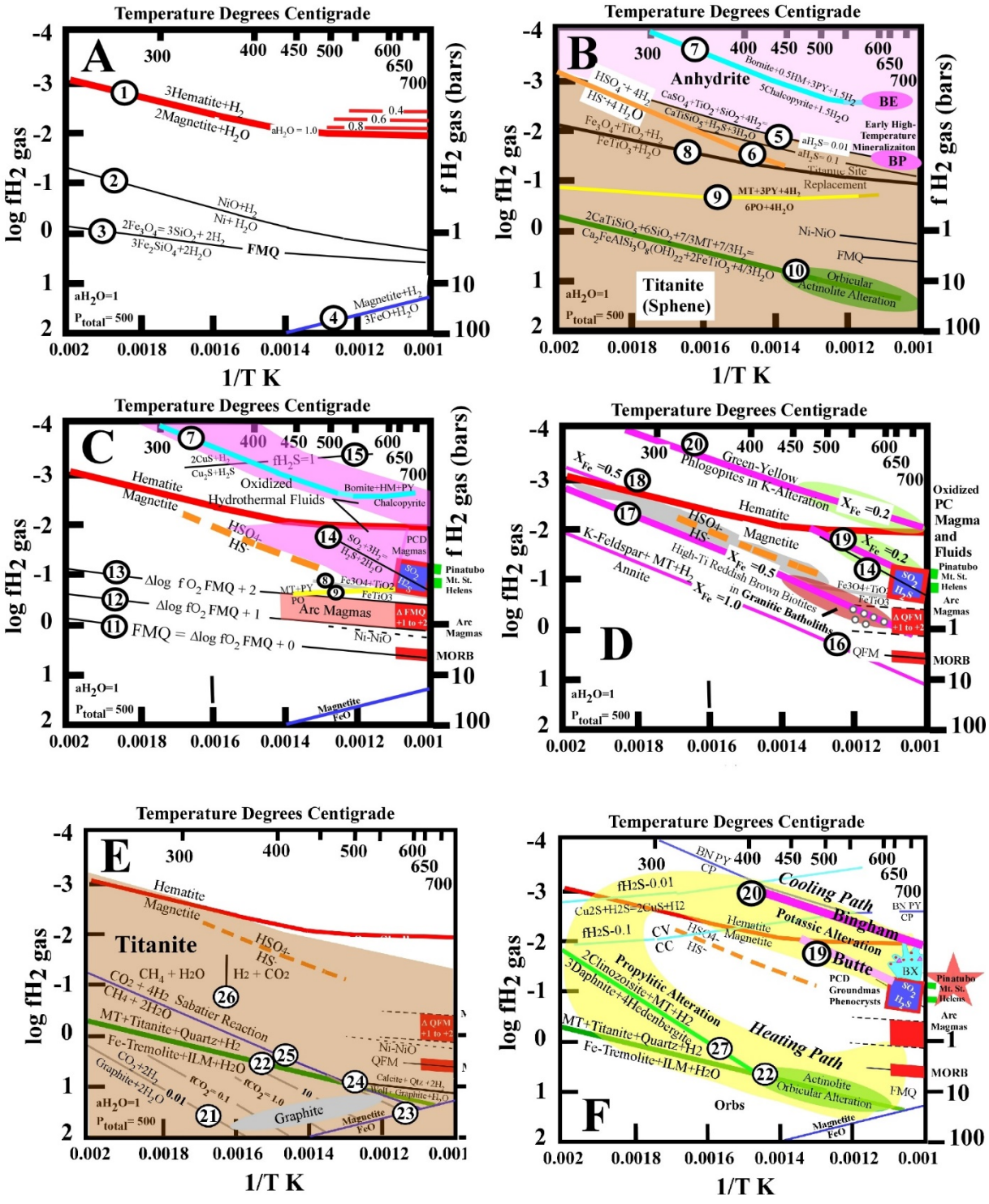

Figure 3. A. Isobaric (500 bars, 50 MPa) polythermal Van't Hoff plot with horizontal axis 1/T K absolute temperature relative to absolute zero with corresponding temperature in degrees Centigrade shown across the top of the diagram. Vertical Y-axis is log fugacity H_2(gas) rather than log K in standard Van't Hoff plots. This figure shows the stepwise construction of this new phase diagram. **A**. Four conventional redox buffers are plotted in terms of logfH_2. **B**. The redox

space is subdivided into two distinct parts: an upper oxidizing region colored pink where anhydrite occurs and a lower reduced region where titanite occurs colored brown. The boundary is near the transition from reduced sulfur in the form of HS^- to oxidized sulfur occurring as HSO_4^-. **C**. Shows a spectrum of well-known magma types with increasing oxidation state from MORBs, to arc magmas, to ore-forming porphyritic magmas and primary anhydrite-bearing strata volcano volcanics including Pinatubo which plot inside the blue-colored box which represents magmatically-derived water which becomes the ore-forming hydrothermal fluids. D. Shows the distinct types of biotite which become progressively more magnesian (less iron rich) with increased oxidation. Miariolytic cavities are shown diagrammatically as a group of small circles along Line "17". While these represent localized saturation with magmatic water, they do not indicate escape of that water as a free ore-forming phase. **E**. Shows as a green line the distal orbicular actinolite-titanite alteration discovered at Bingham Utah and mapped at the Clementine prospect in Montana in relation to even more reduced mineral assemblages with graphite as at the Ruby graphite deposit in Montana. The thermodynamic properties of Fe-Tremolite are used for actinolite as both are Fe-rich amphiboles, as none are available in the SUPCRT data base for actinolite. **F**. Shows the full repeating convective cycle of fluids in yellow starting with out-gassed fluids from a porphyry magma through 3 stages: (1) magmatic H_2 release by oxidative dehydrogenation, (2) sulfide mineralization during cooling once fluids leave the thermal influence of the crystalizing magma and densify, (3) heating as the return flow fluids approach the pluton and become buoyant, and finally (4) distal propylitic alteration occurs with actinolite forming.

The stoichiometry of all the chemical reactions described below which involve H_2 gas as a key geochemical variable are determined by computing balanced oxidation and reduction equilibria of iron and hydrogen; sulfide (S^{2-}) and oxidized sulfate states (S^{6+}) and S ($^{4+}$); carbon dioxide (C^{4+}) and graphite (C^0). For consistency, all reactions are written so as to be exothermic, that is to have a negative Δ Enthalpy of reaction. In **Figure 3 A** the equilibria of hematite (Fe_2O_3) and magnetite ($FeO \bullet Fe_2O_3$) shown by the line "1" provides a useful example in Equation 1.

$$3Fe_2O_3 + H_2\,gas = 2Fe_3O_4 + H_2O \qquad (1)$$

First, the number of moles of iron is balanced with a total of six on both sides. In terms of the valences of iron, the left-hand side of the reaction has a total of 6 ferric ions while the right-hand side has two ferrous ions and four ferric ions since magnetite contains iron in both valence states and can be expressed as $FeO*Fe_2O_3$. The overall or net ionic changes are $2Fe^{3+}$ of the 3 Fe^{3+} in hematite being reduced to $2Fe^{2+}$ in magnetite. This oxidation is balanced by one H_2 or two H molecules becoming oxidized to $2H^+$ in water.

In terms of electron conservation, the hematite- magnetite reaction is the sum of two half-cell equilibria:

$$2Fe^{3+} + 2e^- = 2Fe^{2+} \qquad (2)$$

$$H_2 = 2H^+ + 2e^- \qquad (3)$$

The equilibrium constant is given in equation 4.

$$K_{HM\text{-}MT} = a\,H_2O / fH_2gas \text{ or } \log K_{HM\text{-}MT} = \log aH_2O - \log fH_2 \qquad (4)$$

By setting the aH_2O to 1, then log aH_2O becomes 0, and log fH_2 is equal to - log $K_{HM\text{-}MT}$.

H_2 Fugacity as the Principal Geochemical Variable Assuming the Activity of H_2O Equals One in Hydrothermal Fluids

Here, rather than compute R_H, an explicit expression is calculated which yields an expression of hydrogen fugacity by assuming that the *activity* of water is one. Rather than use R_H here we set the activity of water to unity in all the calculations of hydrothermal equilibria which follow. While this is clearly is an assumption, it is evident from the presence of ubiquitous fluid inclusions in vein quartz and other minerals that porphyry copper hydrothermal systems are wet and water-saturated. Within the constraints of the assumption that the activity of H_2O equaled 1, then setting aH_20 =1 reduces the number of variables thus making it possible to calculate the log fH_2 as the principal variable of interest within the water-rich compositions. While the values of log fH_2 calculated in this fashion are approximate, they are sufficiently accurate to reveal the essential topology of the phase equilibria involved. It is unlikely that the activities of water in nature vary enough from a value of 1 that the essential topology of Figures 3A through F would be dramatically different.

Redox Buffer Assemblages

Figure 3 A shows four of the major redox buffer equilibria commonly used in geochemistry and petrology as lines “1”, “2”, “3”, and “4.” Of these the Fayalite-Magnetite-Quartz line “3” abbreviated “FMQ” is fundamental to characterizing the variation in redox states of certain magmatic systems including parental magmas for porphyry copper deposits and tectonic arc magmas as well. Together all these equilibria span six orders of magnitude of log fugacity H_2. What is different from the values shown here extending from -4 to +2 is that these values are far higher than the log fO_2 values commonly used in petrology which range from -11 to -30 (Eugster and Wones, 1962). Hydrogen gas is an actual gas phase present while oxygen is not. The fact that H_2 is present is evident on the right on axis of Figure 3A where the values of fH_2 are labeled in bars. Of the 500 bars total confining pressure, up to 100 bars are due to the presence of hydrogen proving that H_2 represents up to one fifth of the total pressure especially in the lower parts of Figure 3A which is the reducing end of the spectrum. In contrast, the top of Figure 3A is the oxidizing end.

Effect of Water Activity Less than Unity on the Equilibrium Lines Plotted

Notice that the equilibria for Lines “1”, “2”, “3”, and “4” all involve water (H_2O). The thermodynamic calculations shown here and throughout the rest of this paper set the aH_2O to 1.0. By stipulating that the aH_2O is 1.0, fH_2 can be computed as one algebraic unknown has been eliminated from the equilibrium constant expression. The impact of water activities departing from 1.0 are contoured in Figure 3A for the hematitie-magnetite equilibria Line “1.” Lines for water activities of 0.8, 0.6 and 0.4 are shown. The effect of water activities departing from a value of 1.0 on the other reactions in this study are of identical magnitude since the

stoichiometric coefficients of H_2 and H_2O are the same but of opposite sign with two exceptions. First, in a few reactions in later sections which involve H_2S as a variable besides H_2 and H_2O, departure of the computed lines may vary differently depend on the magnitudes of the stoichiometric coefficients of H_2, H_2O, and H_2S. Second and far more importantly, all reactions with biotite contain hydrogen so that H_2O does not appear in the equilibria. Hence, the lines drawn for reactions with biotite (Figures 3C and 3D) do not vary with H_2O activity. Given the fact that hydrothermal fluids are mostly water, the deviations from unity in nature should be well within the width of this band even for brines with large total dissolved solids (TDS). Furthermore, the lines shown will deviate in the same direction so that the lines shown all move together. Therefore, the departure of aH_2O from unity should not change the general topology of the phase diagram calculated in this study in Figures 3A through F.

Sources of the Mineral-Solution-Gas Equilibria Used

Lines “1”, “2”, “3”, “4” and “16” all involve equilibria containing H_2 investigated earlier by Eugster and Wones (1962) where hydrogen gas was used to (1) control and buffer the desired oxygen fugacity inside platinum capsules where the experimental charge was located and (2) eliminate hydrogen embrittlement of the steel high pressure vessel by encapsulating the platinum capsule within a gold capsule through which H_2 diffusion was impossible. This innovative nested capsule method of Eugster and Wones was focus on determination of the compositional variation of biotite solid solutions under different oxygen fugacities as $\log fO_2$ was considered the primary measure of redox in rocks and has been widely used ever since. Here the focus has changed from $\log fO_2$ to $\log fH_2$. Lines “5” through “28” with the one exception of Line “16” are all developed for this study with a focus on H_2 as the primary variable of scientific interest rather than a necessary experimental parameter to control O_2 and protect equipment as in the Eugster and Wones study of 1962.

While earlier investigators could have chosen to use H_2 rather O_2 to express redox states, there are three reasons why this was not the case and why the preference for O_2 has persisted for sixty years. First, log fO_2 has long been the choice of geochemists to express redox state in ore deposits (Holland, 1959, and Meyer and Hemley, 1967). Second, the ease of use of the Buddington and Lindsey (1964) geothermometer provides both temperature and calculated equilibrium O_2 fugacity independent of having to know the activity of water. Petrologists have retained this convention focusing on $\log fO_2$ since no assumption about the activity of water is necessary to derive a value for $\log fO_2$.

Sulfide Mineralization and Related Alteration Reactions: Magmatic Water Redox State

Figure 3B adds sulfur to the system and line “5” represents anhydrite-rutile-quartz-titanite (sphene) assemblage which subdivides the entire space into the upper pink oxidizing region where anhydrite ($CaSO_4$) is present and the lower reducing region colored brown where titanite or sphene ($CaTiSiO_5$) is present. The boundary between the anhydrite and titanite domains in this figure is closely related to Line “6” representing the iso-fugacity line of HS^- and HSO_4^- separating sulfur in reduced form (value -2) below the line and oxidized value (+6) above the line. This sulfide to sulfate line is also discernible in rare cases in volcanic rocks which have

primary igneous anhydrite which are central to the arguments made herein Figure 3C labeled Pinatubo in green.

The temperature range of early high-temperature sulfide mineralization in porphyry copper deposits is known from fluid inclusion homogenization upon heating using a heating-freezing microscope stage and from a variety of mineral geo-thermometers. The pre-Main Stage at Butte formed between 550-650 degrees C. (Brimhall, 1973 and 1977; Roberts, 1973). Line "7" is the equilibria of copper ore minerals chalcopyrite and bornite- another major recognizable feature in ore deposits. Point "**BP**" represents the early high-temperature sulfide mineral assemblage at Butte Montana which lacks bornite but has a chalcopyrite-pyrite-magnetite-hematite assemblage (Brimhall, 1977) and is responsible for widespread biotitization of hornblende (Brimall et al, 1985). Point "**BE**" represents the early high-temperature sulfide mineral assemblage at Bingham Utah where bornite is included in the early sulfide high-temperature ore mineral assemblage (Einaudi et al, 2003).

Anhydrite and titanite have a central importance in interpreting early high-temperature hydrothermal processes and constraining the composition of fluids from which sulfides formed. Anhydrite represents oxidized fluids with sulfur in its highest valence + 6 state and is ubiquitous in early high-temperature sulfide ores. Titanite is present in many igneous rocks as a common accessory mineral and can be radiometrically dated using U/Pb methods. It has in addition two more important features. Titanite has also been shown to form as a hydrothermal mineral within distal actinolite orbicular alteration (Brimhall, 2018; Brimhall and Fanning, 2019; Brimhall, 2021) and can be radiometrically dated, thus providing two possible age dates, one for magmatic crystallization and another for related hydrothermal activity. Finally, when primary titanite in an igneous rock becomes altered under early-stage hydrothermal processes, the titanium combines with iron to form complex secondary mineral assemblages which can be used to constrain the chemical composition of the fluid precisely as shown by line "8" representing the titanite site replacement equilibria with magnetite, rutile, and ilmenite (Roberts, 1973 and 1975). Notice the proximity of line "8" to line "6" for the HS^-/HSO_4^-boundary. Line "9" represents the pyrite-magnetite-pyrrhotite boundary. Below this line, pyrrhotite is present rather than pyrite. In contrast, the orbicular actinolite assemblage shown by line "10" contains pyrrhotite, chalcopyrite, and ilmenite formed under conditions with very reducing conditions with a high fugacity of H_2.

fO2 Redox Buffers, Arc Magma Reference Frame, and Oxidized Ore-forming Fluids

In order to ease the transition from using fO_2 to fH_2 the common petrological redox buffer Quartz-Fayalite-Magnetite (QFM) is recalculated in terms of H_2 assuming the aH_2O =1 and is shown in Figure 3C. QFM is shown as line "11" and Ni-NiO is dashed. Hematite-Magnetite is shown as a heavy solid red line. Several key magma types of importance in igneous petrology and ore genesis are shown in order to anchor this new figure with respect to a broad understanding of magma genesis in relation to plate tectonic regimes where porphyry copper deposits form often nearby to arc-related strata-volcanoes. This association is at the heart of the "Systems" approach to exploration which includes the full chain of metal enrichment processes involved from source to final ore deposit are considered. The start of this chain is metallogenic fertility of the region where magmas form by partial melting within the mantle wedge above

subduction zones. Line “11” represents FMQ (Δlog fO_2= 0). On the right-hand side of Figure 3C is a small red box labeled MORB standing for Mid Ocean Ridge Basalt formed at spreading centers in ocean basins. In comparison, on continental margins where subduction occurs these sea floor slabs move away from the spreading ridges where MORBs form and descend into the mantle including the MORB basalts and the entire sedimentary sequence deposited over time on top of them. Oxidation of down-going slab complex (MORB slabs and overlying sediments) occurs by several mechanisms. Metamorphic devolatilization of (H_2O, H_2, CH_4, and H_2S) from subducted slabs and their sedimentary cover rocks generates aqueous fluids that ascend upwards into the mantle wedge, inducing the partial melting that produces arc magmas by lowering the melting temperature. These volcanic arc magmas have oxygen fugacities some 10 to 1,000 times higher than magmas generated at mid-ocean ridges since oxidized sedimentary rocks are subducted along with the MORBs (Ague et al, 2022) and slab-derived devolatilization fluids are oxidized by subducted metasedimentary rocks. Another cause of oxidation (Bruce Marsh, personal communication) takes place in the oceanic crust as it moves away from the ridge axis and is highly altered by ongoing hydrothermal convection with sea water which is sulfate-rich—changing the initial $^{87}Sr/^{86}Sr$ ratio from the 0.7025 at the ridge to 0.7035 or more by the time it becomes subducted. Arc magmas may come directly from this altered oceanic crust.

These subduction-related “arc” magmas which are the parental plutons for porphyry copper deposits (Richards, 2015) are generally described as having a redox value of delta log fO_2 of +1 to +2 relative to the FMQ buffer. Lines “12” and “13” show these delta logfO_2 values re-calculated into logfH_2 values defining a pink-colored box labeled “arc magmas.” While such magmas have crystalized by 700 degrees C, this box is bounded by the extrapolated mineral equilibria lines involved. Line “14” represents the iso-fugacity boundary of H_2S and SO_2. Notice a small blue box outlined by red labeled SO_2/H_2S located immediately above Line 8 for the Titanite replacement assemblage (Magnetite-Rutile-Ilmenite) of Roberts (1973). This box is interpreted here to represent the composition of ore-forming magmas and their exsolved magmatic water which have been oxidized relative to arc magmas by continued hydrogen outgassing to the extreme levels required for ore genesis. Notice that this box plots near the anhydrite/titanite boundary and within the anhydrite stability field and is positioned right above the magnetite-rutile-ilmenite line “8”. This fluid composition is critically important as it is the starting point for early high-temperature mineralization and alteration in porphyry copper deposits.

The upwards oxidative sequence of the red-colored boxes on the right-hand edge of Figure 3C is key to understanding the origin of highly evolved ore-forming magmas which starts with MORB basalts, their subduction and oxidation, partial melting of hanging wall mantle which creates oxidized arc magmas and their continued oxidation to form ore-forming magmas- all with continued hydrogen out-gassing called oxidative dehydrogenation.

Since this blue box outlined in red is a key composition of hydrothermal fluids exsolved from ore forming magmas in porphyry copper genesis, its hydrogen fugacity is important to understand. Notice that the logfH_2 value is -1.0 which implies an H_2 partial pressure of about 0.1 bars out of a total pressure for this calculation of 500 bars for this calculation. While this shows that H_2 is not a major component of the total confining pressure, H_2 is indeed an important minor component and is present as a gas. Unlike O_2 with a fugacity of 10^{-29} at 700 degrees C.

Role of H_2 Bubbles in Oxidation and Reduction

In addition to outgassing from magmas causing oxidation of the remaining melt, H_2 which has low solubility in water becomes free to physically migrate in mass. Such migration is not by diffusion, but rather as tiny bubbles transported by advecting water escaping from magma once fluid saturation occurs. Transport of H_2 bubbles in the fluid phase occurs when the rate of fluid advection overcomes the buoyancy of the individual bubbles (Bruce Marsh personal communication). This is the case with tiny bubbles. **Figure 3C** thus helps confirm and more importantly, quantify the assertion that H_2 outgases from magmas and causes their oxidation.

Certain dramatic volcanic eruptions in recent years help visualize this oxidation by H_2 diffusion and ore genesis in general which is normally hidden at depth from human observation. On the right-hand side of the blue-colored box in **Figure 3 C** are two short thick green line segments representing the logfH_2 values computed for two major and now famous volcanic eruptions that contained anhydrite ($CaSO_4$) in their pumices: Mount Pinatubo in 1991 in the Philippines and Mt. St. Helens in the U.S. in 1980. Anhydrite is actually not very common in volcanic eruptions, so the occurrence of anhydrite is viewed in igneous petrology as being very significant and is indicative of rare highly oxidized volatile-rich magmas. The published data for delta logfO_2 from Rutherford (1993) for both these eruptions have been recalculated here to logH_2 values as shown using the equilibria $H_2O = H_2+1/2\ O_2$ setting aH_2O =1.0. Anhydrite occurring as a micro-phenocryst in volcanic rocks has been well-documented and interpreted in two seminal research studies published by Luhr (1982) and Luhr, et al, 1984. Both eruptions were responsible for the massive injection of oxidized (SO_2) sulfur into the stratosphere which lingered for years and may represent the composition of magmatic intrusives equivalent to supergiant porphyry copper deposits (Chiaradia and Caricchi, 2022). In that respect, porphyry magmas have, from a volcanological perspective, been referred to as “failed” mega-volcanic eruptions by Chiaradia and Caricchi (2022) based upon Monte Carlo modeling of the role played by magma injection rates into the upper crust on the formation of porphyry copper deposits with different copper endowments. Their mass balance calculations suggest that supergiant porphyry copper deposits (>10 million tonnes copper) require magma volumes (up to >2500 km3) and magma injection rates (>0.001 km3 year−1) typical of large volcanic eruptions from rift, hot spot, and subduction related settings. However, not all super-giant volcanic eruptions are sulfate-rich. Yellowstone for example is not, but this fact may reflect its mantle hotspot origin. Because large volcanic eruptions would destroy magmatic-hydrothermal systems or prevent their formation, the largest porphyry copper deposits can be considered as failed large eruptions and this may be one of the causes of their rarity. Both mega eruptions and porphyry copper ore deposits are enormous, oxidized sulfur anomalies in the crust driven by comparably energetic magmatic and related hydro-geochemical systems. As Figure 3C shows they both have similar highly oxidized character, well- above normal Arc magmas. The volcanic systems erupt, explode, disperse and dominate the earth’s atmosphere on a planetary scale while the porphyry copper magmas explode, hydro-fracture and convect water at depth on a localized scale which concentrates metals to enrichment factors in excess of 100 times crustal abundances (Brimhall, 1987). For humans living on the Earth’s surface visualization of these anhydrite-bearing eruptions can help convey the massive power released in the subsurface when a porphyry copper deposit forms. In comparison, mid ocean ridge basaltic lavas (MORB) plot along Line “11” and are far less

oxidized and erupt slowly from cracks as witnessed in Iceland today usually without explosions as the magma is less silica rich, and hence far less viscous.

Possible Geochemical Basis for Rare Cataclysmic Mega-Volcanic Stravolcano Eruptions Containing Anhydrite and Porphyry Copper Ore Deposits: Is Hydrogen the Missing Link?

On a comparative basis, the Mt. Pinatubo stratovolcano is the second-largest eruption of the 20th century. The ash plume height reached more than 40 km high and ejected more than 10 km^3 of magma, classifying it as an Ultra-Plinian eruption style. The world's largest eruption of the 20th century occurred in 1912 at Novarupta on the Alaska Peninsula which is also part of the Pacific Ring of Fire where porphyry Copper deposits form at depth. An estimated 15 km^3 of magma was explosively erupted equivalent to 230 years of eruption at Kilauea (Hawaii) or about 30 times the volume erupted by Mount St. Helens in Washington. What aspect of these unusually energetic geochemical systems makes them *both* so explosive? A speculative answer is proposed here- one that at least may explain why so much volcanic ash exploded and why hydrofracturing is so well developed in porphyry systems. With the previous focus on oxygen as the measure of redox state, no explanation is evident for these mega-eruptions in the published literature. However, here by translating the redox metric into a hydrogen frame of reference a possible answer or at least a new factor to consider emerges. One unique aspect of hydrogen stems from its minute molecular size and well-known tendency to weaken structures in contact with it for forming hydrides or weakening mineral strength. It is suggested there is a possible chemical-mechanical effect of abundant hydrogen (Griggs, 1967). Hydrogen gas may have played a major role in the multi-stage fracturing characteristic of porphyry copper deposits and perhaps also in certain volcanic mega-eruptions. Conventionally, over-pressured aqueous fluids are invoked to explain fracture development with release of magmatic water which expands and does pressure-volume work causing brittle rock failure at depths where such expansion is accommodated. The accepted hypothesized mechanism is that the partial molal volume of water in the aqueous phase is far greater than within the silicate melt and causes the proposed expansion. Here a mechanism that may enhance this volumetric expansion is proposed when hydrogen is present as shown in **Figure 3C** and thus may augment the explosiveness of porphyry melts. Hydrogen, recognized herein may dramatically enable the hydrofracturing process through hydrolytic weakening of quartz and other minerals (Griggs, 1967; Rovetta et al. 1989; and Strauch et al, 2023) or embrittlement so that the stress levels required to cause brittle failure induced by water expansion, are dramatically lowered. Hydrolytic weakening and embrittlement of rocks by hydrogen could then significantly enlarge the volume of a hydro-fractured rock mass enhancing convective flow and related alteration and mineralization in porphyries and affecting rock fragmentation at depth necessary for volcanic eruption.

Biotite Mineral Chemistry and Redox

Stemming from the blue box in **Figure 3C** are broad zones shown in pink that represent the composition of oxidized hydrothermal fluids in equilibrium with the oxidized magmas as they cool. Notice that the pink zones are displaced to the right along the Hematite-Magnetite boundary and follow the bornite-chalcopyrite line shown in blue Line “7.” At low values of H_2, this zone passes from the chalcocite field into that of covellite at Line “15” typical of the Advanced Argillic assemblage at temperatures below 400 C.

Figure 3D shows the location of biotite-bearing granitic rock assemblages which are well-known as geochemical sensors of fluid composition (Brimhall and Crerar, 1987, John et al, 2010). Biotite equilibria are used to establish the purple zones in Figure 3C. Since most hydrothermal biotites occur in solid solution containing iron, magnesium, and other elements, we show these phases as their Fe-end member and then illustrate how incorporation of magnesium changes the phase relations using ideal site mixing in annite–phlogopite solid solutions (Brimhall and Crerar, 1987; Ague and Brimhall, 1987, 1988). Ideal site mixing provides a useful substitution where the activity of the annite $KFe_3AlSi_3O_{10}(OH)_2$ component in biotite solid solution equals X_{Fe}^3.

Line "16" is for pure ferrous Fe biotite annite in equilibrium with magnetite and K-feldspar denoted as X_{Fe} =1.0. Line "17" represents the measured average biotite composition in granitic batholiths with a X_{Fe} of 0.5 (Ague and Brimhall, 1987, Ague and Brimhall 1988a and b). These igneous biotites are distinctly reddish brown in color under the petrographic microscope and have elevated TiO_2 contents up to 4.5 weight percent responsible for the brownish color. Networks of tiny acicular rutile grains are often observed exsolved into the basal 001 plane of these micas illustrating the intrinsic instability of such high-Ti biotites. A gray colored zone is shown surrounding "Line 17" representing the lowest oxidation state of typical granitic batholiths. These rocks then serves as regional-scale redox buffers as within the Butte Granite thus keeping early high-temperature fluids from becoming more reduced and forming actinolite orbs.

Line "17" is displaced to the right to Line "18" where it crosses the hematite-magnetite boundary. Lines "17 and 18" are typical of primary igneous biotites formed within thousands of plutons that occur within batholiths like the Sierra Nevada or the Boulder batholith as part of the Pacific Ring of Fire formed along a convergent tectonic plate boundary. Saturation with magmatic water and fluid escape which quenches the melt is very rare yielding a porphyritic texture. In contrast, the norm is slow cooling which causes an equi-granular texture. Miarolytic cavities are shown diagrammatically in **Figure 3-D** as a group of small circles on Line "17." While these represent localized saturation with magmatic water, they not coalesce nor do they indicate escape of that water as a free ore-forming phase. Hence, in general plutons with miarolytic cavities do not constitute ore-forming magmas which instead, yield magmatic water en mass once hydrofracturing initiates. In comparison, many hydrothermal biotites formed from such ore-forming fluids are pale greenish to yellow in color in thin section and have far less titanium than igneous biotites. Hydrothermal biotites occur along Lines "19" and "20" labeled X_{Fe} =0.2. Notice that these lines are also displaced to the right across the Hematite-Magnetite boundary.

Reduced H_2-Rich Mineral Assemblages: Orbicular Actinolite Alteration and Occurrences of Grapihte

Figure 3E shows in brown color the expanse of the titanite stability field formed under reducing, high fH_2 conditions contrasting sharply with the stability field of anhydrite shown in pink in Figure 3B. Line "21" shows the Graphite-CO_2 boundary for an fCO_2 of 0.01. This line migrates to the right as the fCO_2 increases. Note that Line "22" demarking the equilibria of the actinolite (calculated here using Fe-Tremolite its thermodynamic properties) orbicular alteration

is in the vicinity of the graphite-CO_2 equilibria shown in gray when the fCO_2 has a value of 10 bars which is similar to the fH_2 at a temperature of approximately 450 to 550 C. This association of graphite with actinolite calcite orbs was vividly borne out in the field when Neil Griffis of the USGS made a discerning discovery of graphite near the type section of actinolite orbs on Parker Creek (Figure 2). The Sabatier Reaction (Line "25") predicts that at such elevated temperatures, CO_2 and H_2 would be the dominant species. The rock sample analyzed by ALS Global showed 13 percent total carbon using infrared spectroscopy (IR) and after HCl leaching, showed over 2 percent graphitic carbon remaining detected by IR spectroscopy and confirmed by optical mineralogy in polished thin section.

This association of graphite with amphibole-bearing assemblages is also consistent with the fact that the Ruby Mine flake graphite deposits southeast of the Dillon (Bell, this volume) have amphibolite wall rocks nearby (James, 1990) as well as marbles. If the source of fluids that caused graphite to form came from magmas then Figure 3E implies that the fluids were very reducing and had a very high fH_2, perhaps similar to those shown as Mid Ocean Ridge Basalts (MORBS) in the red box on the FMQ line on the Y-axis, or other mantle-derived highly reduced mafic magmas. Serpentinized ultramafic rocks are known to have a redox state even lower near Magnetite-FeO shown as line "23" directly below Line "24" representing hydrothermal reduction of calcite by H_2 in the presence of quartz. Salotti, and others, 1971 proposed an abiotic mechanism for the formation of graphite with the carbon being supplied from the carbon in pre-existing carbonate minerals. The carbon is released by direct methanation through a reaction with elemental hydrogen. The subsequent pyrolysis of methane releases elemental carbon (Salati, and others, 1971). Similarly, Galvez and others, (2013) concluded that graphite may form by carbonate reduction during subduction and Rumble and Hoering (1986) presented evidence of hydrothermal graphite genesis.

Sabatier Reaction and H_2 and CO_2 in Porphyry Copper Ore-forming Fluids

Line "25" in **Figure 3E** demarks the position of the well-known Sabatier Reaction shown here for an iso-fugacity of CO_2 and CH_4 and an activity of H_2O equal to one. The value of the equilibrium constant for this reaction changes sign at about 350 degrees C. Above 350 degrees C. to the right of the vertical Line "26" the favored species are H_2 and CO_2. Fluid inclusions in the early high-temperature stage of porphyry copper deposits often have CO_2. However, H_2 to date has not been noted. Mavrogenes and Bodnar (1994) showed experimentally that H_2 readily diffuses through quartz which is the most common host for fluid inclusions and concluded that "hydrogen will diffuse out of inclusions if the inclusion-bearing sample is exposed to conditions significantly different from those in the inclusions." The rapid diffusion of H_2 into fluid inclusions in quartz was consistent with the diffusion rate constants measured by Kats et al, 1962. From this work it is clear that H_2 will diffuse through many rocks whenever a H_2 concentration gradient exists. Therefore, it is not surprising that while the thermochemical results presented here prove a substantial H_2 concentration in ore-forming fluids, H_2 has not been recognized as a common constituent in fluid inclusions as it is probably a largely fugitive species. The only lasting evidence of the migration of H_2 in porphyry copper deposits is then likely to be the recurrent mineral assemblage supported by theoretical chemical phase equilibria from which fluid composition is computed. The mixture of molecular hydrogen and carbon

dioxide which is favored by the Sabatier reaction above about 350 C together constitute a powerful agent for reduction.

Cycling of H_2 by Convection in Butte and Bingham Type Systems: Cooling and Heating Paths

Finally, shown as a yellow-colored arc in **Figure 3F** the cooling and heating portions of the convective cycling of H_2 proposed here for two distinct types of PCD deposits: Butte (Line 19) and a more oxidized system at Bingham (Line 20) shown as BP and BE in Figure 3B respectively. These heating paths *point upwards to the left.* For Butte, the initial hydrothermal fluid escapes from the blue box along Line 14 (Figures 3 C and D) which is similar to the redox state of oxidized Pinatubo arc magmas with anhydrite. As H_2 on the right-hand side of Line 14 escapes from porphyry copper magmas as minute bubbles carried in early high-temperature fluids, Le Chatelier's Principle drives the reaction to the right creating more SO_2. Biotitic breccias formed explosively on the tops of Butte porphyry dikes are shown in the light blue zone labeled “BX.” At Butte, the only early sulfides to form are chalcopyrite and pyrite without bornite. With cooling, the path along Line 19 intersects the magnetite-hematite line. At lower temperatures around 300 C chalcocite and covellite form where the early-stage buffer with magnetite-K-feldspar-biotite is destroyed by sericitic and advanced argillic alteration. At Bingham in contrast, which formed along a higher oxidation state, Line 20, the early-stage sulfides are chalcopyrite, pyrite and bornite formed along Line 7 as shown in Figure 3B.

The heating paths shown in **Figure 3F** are shown in green *pointing downward to the right* and consist of the equilibria of propylitic alteration “Line 27” and the actinolite orbicule assemblages shown as “Line 22.” It is known that convective hydrothermal cells develop at the top of ore-forming magmas driven by the temperature gradients between the hot but cooling plutons and the surrounding wall rocks (Norton and Knight, 1977). The shape of the convective systems are elliptical toroids. This means that the cooling paths shown in **Figure 3F** connect with the return heating paths as a convective loop shown in gray.

Timing and Duration of Hydrogen Gas Release from Magma

While bubble accumulation and magmatic vapor transport (MVP) has been modeled by Parigiani and others 2016 and 2017 and Gruzdeva and others (2024), the volatile species considered are H_2O, CO_2, S, Cl, F, Li, B, and noble gases but not H_2 in particular. While all these gas species are important in ore genesis, it has been shown here that H_2 has an unequaled influence on oxidation and reduction. Nevertheless, modeling by Parigiani and others 2016 and 2017 and Gruzdeva and others (2024), show that ore formation from hydrous magmas may involve distinct phases of volatile release. “Magma convection at early melt-dominated states leads to homogenization, which delays fluid release and promotes a rapid evolution toward a mush state. Subsequent onset of magmatic volatile release can be near-explosive with a tube-flow outburst event that could result in the formation of hydrothermal breccias and vein stockworks or trigger eruptions. This event can be followed by sustained fluid release at moderate rates by volatile flushing caused by magma convection.”

Volcanic Eruptions Containing Anhydrite and Their Parallel with Porphyry Copper Deposit Magmas

Luhr (2008) summarized global volcanic eruptions containing primary igneous anhydrite extending as far back as 1948 and provides a detailed description of micro-phenocrysts of anhydrite co-existing with pyrrhotite and titanite in fresh pumices in the 1982 eruption of El Chichon, Mexico as well as in the far larger eruption at Mt. Pinatubo in 1992 in the Philippines which is a Mega-Strata Volcanic Eruption. Coexisting anhydrite and titanite is consistent with the highly oxidized state implied in Fig. 3B, Line 5 and Fig. 3D for Mt. Pinatubo shown as green lines. Luhr cites anhydrite crystallizing from the melt during the final stages of crystallization prior to eruption, noting glass inclusions within anhydrite crystals as the strongest evidence in favor of direct crystallization of anhydrite from the melt. The high content of water, incompatible trace elements, high K_2O, high sulfur as SO_3, presence of titanite and high calculated log fO_2 far in excess of Ni-NiO, and porphyritic texture shows a similarity with porphyry copper magmas and points out also that El Chich6n is within the regional PCD metallogenic belt in Mexico. The water and gas- saturated condition and calculated depth of 9 km are also similar to PCDs including Butte, Montana. Most revealing is the “excess gas release” phenomena of 5–9 million tons of SO_2 released to the stratosphere by the El Chich6n eruption and larger “excess gas release” of ~20 million tons of SO_2 for the significantly larger eruption of Mount Pinatubo.

Fluid Circulation Cell

In **Figure 4** an ideal advective circulation cell with an elliptical torus shape is shown surrounding a central pluton. Potassic alteration occurs within and slightly outside of the pluton. Anhydrite shown in pink occurs within the Potassic alteration zone. At Butte Montana where the ore body occurs within the Butte Granite wall rock, a zone of biotitized hornblende demarks the Potassic zone which dies out upwards where the granite contains unaltered titanite and hornblende in fresh granite. Stockworks and biotite crackle veinlets also die out upwards. In Bingham-type systems, the potassic zone is surrounded by an actinolite-titanite-calcite ring shown as green dots surrounded by a Propylitic zone shown in green color. The distal actinolite orbs are shown as green dots which form an annular shell surrounding the convective system thus appearing like a bulls-eye target in plan view. This distal ring of orbicular actinolite is easily recognized in the field and is mappable even under dense tree canopy as it is intensely silificified and resists soil-forming processes. This orb ring is absent from batholith-hosted systems like Butte as the granitic rock buffer precludes the redox state from descending low enough to form actinolite orbs.

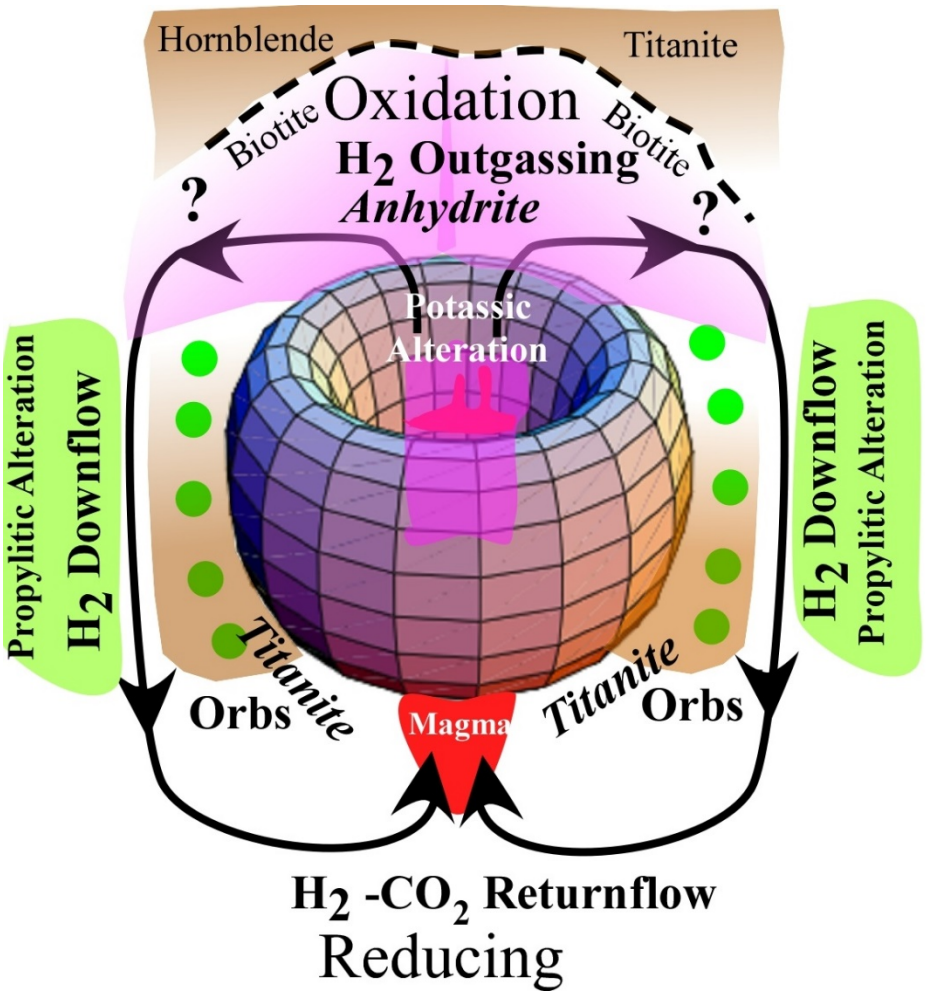

Figure 4. Elliptical torus fluid flow geometry around a cooling pluton for porphyry copper deposits. Actinolite orbicular alteration is shown diagrammatically in cross section as distal green dots inside of the rocks containing titanite shown in brown. In the central upper part of the system, titanite is not stable and anhydrite occurs instead shown in pink. On the very top of the early high-temperature system titanite is again stable in granitic wall rocks above a zone of biotitized hornblende.

An Operative Porphyry Copper Model

The tube flow outburst followed by sustained fluid (including H2 gas) release in combination with the thermochemical mineral assemblage analysis provided here can together be assembled into an operative porphyry copper model. A thermodynamic diagram is developed here for redox equilibria in porphyry copper genesis presented in **Figure 5**. The H_2 vs 1/T Van't Hoff reference frame at water saturation works as an operative geochemical diagram because confined-flow migration of H_2 by magmatic outgassing and thermal advection causes oxidation by dehydrogenation and reduction in the regions where H_2 concentrates along the return flow heating path approaching the pluton. Two concentric advective circulation cells emerge in the log H_2 vs. 1/T space. The largest advective circulation cell shown as black arrows surrounding a yellow zone defines sediment-hosted Bingham-type PCD systems which reach both extreme early oxidative states with chalcopyrite, bornite and digenite (chalcocite) and extreme reductive

states with distal actinolite orbicular alteration. Expulsion of highly oxidized early high temperature aqueous fluids continue to lose H_2 and oxidize along a cooling path defined by the Mg-rich (X_{Fe}=0.2), Ti-poor hydrothermal biotite-magnetite-K-feldspar Potassic alteration mineral assemblage line which serves as definitive trajectory of the cooling pathway. The return heating pathway is demarked by Propylitic alteration and distal actinolite orbicular alteration. In contrast, the batholith-hosted Butte-type PCD cell shown as blue arrows surrounding a gray area has a narrow limited early oxidation range which does not extend up to bornite or digenite and consists only of chalcopyrite-pyrite. It also lacks a distal orb ring due to restrictive chemical buffering by the influence of granite wall rocks with red-colored high-Ti (X_{Fe}=0.5) biotite terminating in the advanced argillic assemblage with covellite and chalcocite on the oxidized end where intense sericitic and advanced argillic alteration destroys the granite buffer. Occurrences of actinolite orbs at Bingham, Escondida, El Hueso, Cajamarca, Morenci, Fortitude, Cananea, and Oyu Tolgoi imply that an actinolite orb ring may be a definitive indicator of large PCD systems. Given the necessity of electron conservation, a large actinolite orb ring portends a large highly-oxidized Potassic alteration zone with chalcopyrite, bornite and digenite. This exploration target size indicator supported by H_2 dynamics and redox thermochemistry may provide focus and help guide discovery of new deep confined PCDs of considerable size and is being tested at the Clementine prospect in southwest Montana which has a 3 by 5 km orb ring.

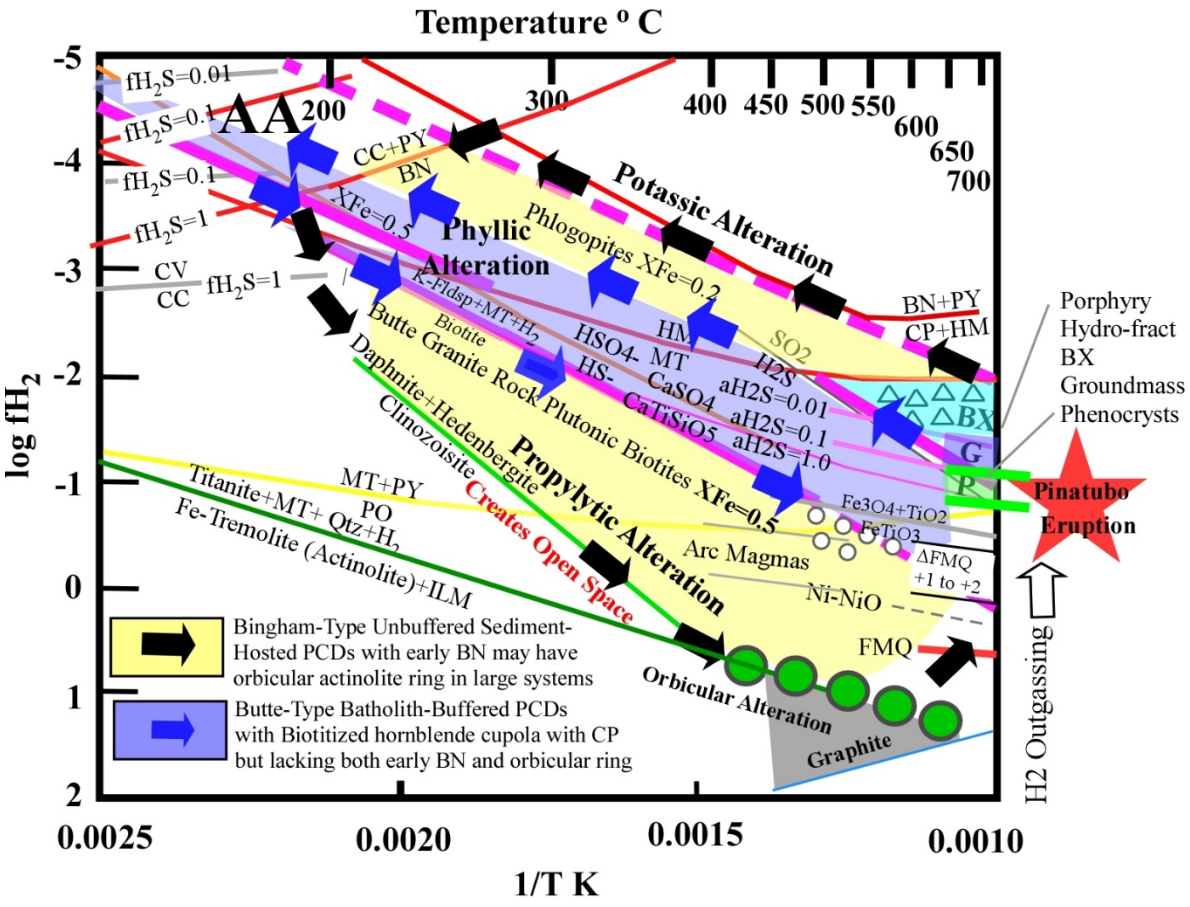

Figure 5. An operative porphyry copper model is shown. Two concentric advective circulation cells are shown with arrows. Confined-flow hydrogen bubble migration by magma outgassing

and thermal advection causes oxidation where de-hydrogenation occurs and reduction along the return flow heating path approaching the pluton where hydrogen accumulates. The larger cell shown with black arrows defines Bingham-type systems which attain both extremely high early oxidative states with chalcopyrite, bornite and digenite and extreme reductive states with propylitic and finally orbicular actinolite alteration. In contrast, the smaller batholith-hosted Butte-type porphyry Cu cell shown with blue arrows has a narrow limited early oxidation range which consists only of chalcopyrite-pyrite. It also lacks a distal orb ring due to restrictive chemical buffering by the Butte granite wall rocks with high-Ti (X_{Fe}=0.5) biotites. This cell extends up to the advanced argillic assemblage with covellite and chalcocite by cooling while the heating path causes propylitic alteration with epidote as the upper shell above biotitized hornblende. Conventionally, water saturation in magmas creating over-pressured fluids is invoked to explain fracture development by violent release of magmatic fluids which expand and cause explosive brittle rock failure. Here I assert that hydrogen diffusion, may dramatically enhance the fracturing process through hydrolytic weakening of quartz and other silicate minerals. Hydrolytic weakening by H2 may also explain why the few springs on the Clementine prospect all occur only within or very near orb alteration zones. Finally, H_2 diffusion may also cause hydrolytic weakening of the carapace which confines deep porphyry systems. Hydrogen may be a part of vapor saturation at great depth of 7 to 9 km noted by Jim Luhr for the El Chichon and Mt Pintatubo volcanoes which both had primary igneous anhydrite and released tens of millions of tons of SO_2. As the threshold required for overpressure fracturing is lowered, a cataclysmic strata-volcanic eruption containing anhydrite may occur as a destructive alternative fate of a deep porphyry copper deposit shown as a large red star.

Proposal of a Target Size Indicator (TSI)

Knowing now that H_2 was in fact present in early high-temperature processes, impacts of this conclusion may have broad potentially useful implications. The distal diffusion-controlled orbicular actinolite (Fe-Tremolite)-titanite-ilmenite calcite assemblages reflect the advective return of H_2 gas to edges of the magmatic-hydrothermal convection cell. Multi-element geochemistry shows that the same hydrothermal fluid was responsible for veins as well as orbs as part of an upright barrel-shaped elliptical torus convection system. Thus, the *oxidative* processes within the central part of a district forming early high-temperature Potassic alteration and related early high-temperature sulfide mineralization must be balanced by the *reductive* processes occurring in the surrounding distal actinolite-titanite-ilmenite alteration zones. If correct, then the inferred district-scale H_2 and electrochemical linkage has important implications for early-stage exploration strategies. The physical dimensions in plan-view of the reduced actinolite orb ring may be forced by H_2 mass balance and electro-chemistry on a convective scale to be at least roughly proportional to the size of the coaxial central zone of oxidized copper sulfide veining. Hence, a potential exploration target size indicator supported by thermochemistry emerges from this use of the hydrogen geochemical perspective.

Conclusions

The H_2 geochemical reference frame adopted here works because it is the migration of H_2 by magmatic outgassing that causes oxidation and reduction in the regions where it concentrates. By

specifying water activity at unity to discover results that are *approximately* correct, several important outstanding questions involving magmatic processes and ore genesis are resolved and a vivid volcanic frame of reference is offered to describe the processes involved. **First**, while earlier studies using the Fayalite-Magnetite-Quartz (FMQ) fO_2 redox buffer have speculated that H_2 degassing may have elevated the oxidation state of subduction-related arc magmas to delta log fO_2 FMQ of + 1 to 2, here formulation of this buffer in terms of fH_2 instead of fO_2, quantifies this assertion that shows that H_2 mobility is indeed the major factor in magma oxidation. This process here referred to a oxidative dehydrogenation is the operational mechanism that has been missing. These oxidized arc magmas have a redox state typical of equi-granular plutons forming batholiths but lacking mineralization. Igneous biotites reflect this redox state with reddish brown color in thin section and high TiO_2 contents around 4 percent. **Second**, ore-forming porphyritic magmas that exsolve water and out-gas H_2 en masse experience extreme oxidation attending early high-temperature Potassic wall rock alteration with titanite destruction and anhydrite formation. Mg-rich hydrothermal phlogophitic alteration in the biotite-magnetite-K-feldspar equilibria define reaction paths parallel to the HS^-/HSO_4^- boundary but directly over the iso-fugacity boundary of H_2S and SO_2. Such oxidized biotities have lost their TiO_2 content and are yellow to greenish in color. **Third**, continued H_2 out-gassing causes continued oxidation of HS^- to $HSO4^-$ which serves as an effective H_2 pump which if structural confinement limits H_2 escape, continues to create hydrothermal fluids rich in H_2 that advect downward along the sides of the ore-forming hydrothermal barrel-shaped elliptical torus convection cell centered on the parental porphyry pluton. **Fourth**, at the high H_2 fugacity caused by H_2 pumping, actinolite (Fe-Tremolite)-titanite-ilmenite assemblages form reflecting the advective return of H_2 gas to distal edges of the magmatic-hydrothermal convection cell. **Fifth**, H_2 movement by district-scale advection requires conservation of electrons as well as hydrogen mass. Thus, the *oxidative* processes within the central part of a district forming early high-temperature Potassic alteration and sulfide mineralization must be balanced by the *reductive* processes occurring in the surrounding distal edge zones. If correct, then the inferred district-scale H_2 and electrochemical linkage has important implications for early-stage exploration strategies. The dimensions in plan-view of the actinolite orb ring are likely forced by electro-chemistry on a convective scale to be proportional to the size of the coaxial central zone of copper sulfide mineralization within the Potassic alteration zone. Hence, a potential exploration target size indicator (**TSI**) supported by thermochemistry emerges from this use of the hydrogen geochemical perspective. Finally, since earning a social license for mining deep ore bodies is based in part on the public's understanding of ore genesis, a vivid example of the hydrogen recycling model proposed here is provided by the eruption of Mount Pinatubo in 1991 in the Philippines which contained phenocryst anhydrite and a magma similar to the highly oxidized melts in porphyry copper deposits. Envisioning how a rare energetic mega-strata volcanic eruption containing anhydrite may represent a once-potential porphyry copper deposit that was not confined at depth but instead exploded and erupted cataclysmically may provide a useful public outreach model as it offers tangible evidence of the size of these systems and the energy levels involved.

Acknowledgements

Kaleb Scarberry is thanked for organizing the scientific program. Chris Gammons and Kyle Eastman provided insightful reviews of this manuscript. The late Jim Luhr is recognized for

inspirational insights in volcanism, mastery of petrological methods that revealed the importance of anhydrite in volcanic rocks, and for shared excitement and engaging friendship. Jeff Dick, is acknowledged for his CHNOSZ computational package and mineralogical thermodynamic data base that make all the thermodynamic calculations presented here possible. Jay Ague and Bruce Marsh are thanked for numerous enlightening discussions of geological processes. Bill Atkinson and Marco Einaudi who recognized and logged the first actinolite orbs at Bingham are thanked for their gracious help to the author after he recognized similar orbs in Montana. Neil Griffis (USGS) is heartedly thanked for his discerning discovery of graphite near the type section of actinolite orbs on Parker Creek. The author thanks all of his colleagues in Clementine Exploration LLC for their abiding interest and support, including Mary Jane Brimhall, Doug Fuerstenau, Ray Morley, Daniel Kunz, Ed Rogers, Bruce Marsh, Abel Vanegas, Chris Lewis, and Tim Teague. Brian Collins kindly provided the mathematical name of elliptical torous used to describe the convective field in three-dimensions. The field work that supports this project starting in 2011 was augmented by the support of neighbors in Wise River and Butte including Dean Stodden, Jim Freestone, Ryan Brown, Don Heffington, Jim Holland, and John Lundborg in shuttling vehicles in support of mapping and helping recover from inevitable vehicle breakdowns. Finally, Erik Torgeson, Licette Hammer, and Jim Freestone of the USFS made environmental regulatory compliance tractable through sharing their considerable expertise and engagement with us in on-going field work.

References

Ague, J.J., and Brimhall, G.H., 1987, Granites of the batholiths of California: Products of local assimilation and regional-scale crustal contamination: Geology, v. 15, p. 63–66.

Ague, J.J., and Brimhall, G.H.,1988a, Regional variations in bulk chemistry, mineralogy, and the compositions of mafic and accessory minerals in the batholiths of California: Geological Society of America Bulletin, v. 100, p. 891–911.

Ague, J., Tassara, S., Holycross, M., Li, J., Cottrell, E., Schwarzenbach, E., Fassoulas, C., and John, T., 2022, Slab-derived devolatilization fluids oxidized by subducted metasedimentary rocks: *Nat. Geosci.* 15, 320–326.

Andersen, D., J., Lindsley, D. H., and Davidson, P. M, 1993, QUILF: A Pascal Program to Assess Equilibria Among Fe-Mg-Mn-Ti Oxides, Pyroxenes, Olivine, and Quartz: Computers and Geosciences, v. 19, no. 9, p. 1333-1350.

Atkinson, W., and Einaudi, M.T., 1978, Skarn formation and mineralization in the contact aureole at Carr Fork, Bingham, Utah: Economic Geology, v. 75, p. 1326–1365.

Brimhall, G.H. Jr., 1973, Mineralogy, texture, and chemistry of early wall rock alteration in the deep underground mines and Continental area, in Miller, R.N., ed., Guidebook for the Butte field meeting of the Society of Economic Geologists: Society of Economic Geologists Guidebook, Anaconda Company, Butte, Montana, p. H1–H5.

Brimhall, G.H., 1977, Early fracture-controlled disseminated mineralization at Butte, Montana: Economic Geology, v. 72, p. 37–59.

Brimhall, G.H, 1979, Lithologic determination of mass transfer mechanisms of multiple stage porphyry copper mineralization at Butte, Montana: Vein formation by hypogene leaching and enrichment of potassium-silicate protore: Economic Geology, v. 74, p. 556–589.
Brimhall, G.H., 1980, Deep hypogene oxidation of porphyry copper potassium-silicate protores: A theoretical evaluation of the copper remobilization hypothesis: Economic Geology, v. 75, p. 384-409.

Brimhall, G.H., 2018, Orbicular alteration at the porphyry copper prospect of southwest Montana: Defining the edges of advective flow in the porphyry copper paradigm: Montana Bureau of Mines and Geology Special Publication 120, p. 71–84.

Brimhall, G.H., 1987, Preliminary fractionation patterns of ore metals through Earth history, Chem. Geol., v. 64, 1-16.

Brimhall, G., 2021, Deep Sediment-Hosted Porphyry Copper Deposits with Critical Mineral Potential and the Geochemical Relationship of Orbicular Actinolite Alteration to District Zoning and Oxidation by Carbonate Dissolution CO2 Release, Montana Bureau of Mines and Geology, Special Publication 123, p. 27-58.

Brimhall, G.H., Agee, C., and Stoffregen, R., 1985, Hydrothermal conversion of hornblende to biotite: Canadian Mineralogist, v. 23, p. 369–379.

Brimhall, G.H., and Crerar, D.A., 1987, Ore fluids: Magmatic to supergene, in Thermodynamic modeling of geological materials: Minerals, fluids and melts, I. Carmichael and H. Eugster, eds.: Mineralogic Society of America Reviews in Mineralogy, v. 17, ch. 10, p. 235–321.

Brimhall, G.H, and Fanning, M., 2019, Supporting the transition to deep porphyry copper exploration: SHRIMP U/Pb radiometric dating of titanite (CaTiSiO5) in the distal and superjacent orbicular alteration zone of the Clementine prospect, southwest Montana: Montana Bureau of Mines and Geology Special Publication 121, p. 117–132.

Cameron, E.N., and Weis, P.L., 1960, Strategic graphite, a survey: U.S. Geological Survey Bulletin 1082-E, 321 p.

Chiaradia, M., Caricchi, L., 2022, Supergiant porphyry copper deposits are failed large eruptions. Commun. Earth Environ. v. **3**, number 107.

Dilles, J.H., and Einaudi, M.T., 1992, Wall-rock alteration and hydrothermal flow paths about the Ann-Mason porphyry copper-deposit, Nevada—a 6-km vertical reconstruction: Economic Geology, v. 87, p. 1963– 2001. Dott, Robert H. Jr., 1992, Eustasy: The Historical ups and downs of a major geological concept: Geological Society of America Memoir 180, 83–91.

Einaudi, M. T., 1977, Environment of Ore Deposition at Cerro de Pasco, Peru: Economic Geology, v. 72, p. 893-924.

Einaudi, M.T., Hedenquist, J., and Inan, E., 2003, Sulfidation state of fluids in active and extinct hydrothermal systems, Giggenbach Volume, Simmons, S.F., ed.: Society of Economic Geologists and Geochemical Society Special Publication 10, p. 285–313.

Eugster, H. and Wones, D., 1962, Stability Relations of the Ferruginous Biotite, Annite: Journal of Petrology, v. 3, p. 81-125.

Galvez, M., Beyssac, O., Martinez, I., Benzerara, K., Chaduteau, C., Malvoisin, B., and Malavieille, J., 2013, Graphite formation by carbonate reduction during subduction: Nature Geoscience, v. 6. June.

Ghiorso, M., and Sack, R., 1991, Fe-Ti oxide geothermometry: thermodynamic formulation and the estimation of intensive variables in silicic magmas: Contributions to Mineralogy and Petrology, v. 108, p. 485-510.

Giggenbach, W. F., 1987, Redox processes governing the chemistry of fumarolic gas discharges from White Island, New Zealand: Applied Geochemistry, v. 2, p. 143–161.

Griggs, D., 1967, Hydrolytic Weakening of Quartz and Other Silicates: Geophysical Journal of the Royal Astronomical Society, v. 14, p. 19-31.

Gruzdeva, Y., Weis, P., and Andersen, C., 2024, Timing of volatile degassing from hydrous upper-crustal magma reservoirs with implications for porphyry copper deposits: Journal of Geophysical Research: Solid Earth, 129, e2023JB028433. https://doi.org/10.1029/2023JB028433.

Guo, S., Bluth, G. J. S., Rose, W. I., Watson, I. M., and Prata, A. J. (2004), Re-evaluation of SO_2 release of the 15 June 1991 Pinatubo eruption using ultraviolet and infrared satellite sensors, Geochem. Geophys. Geosyst., 5, Q04001, doi:10.1029/2003GC000654

Gustafson, L.B., and Hunt, J.P., 1975, The porphyry copper deposit at El Salvador, Chile: Economic Geology, v. 70, p. 857–912.

Helgeson, H.C., Delany, J.M., Nesbitt, H.W., and Bird, D.K., 1978, Summary and critique of the thermodynamic properties of rock-forming minerals: American Journal of Science, v. 287-A, p. 1–229.

Helgeson, H.C., Owens, C.E., Knox, A.M., and Laurent, R., 1998, Calculation of the standard molal thermodynamic properties of crystalline, liquid, and gas organic molecules at high

temperatures and pressures: Geochimica Cosmochimica Acta, v. 62, p. 985–1081, doi: 10.1016/S0016-7037(97)00219-6

Helgeson, H.C., Laurent, R., McKenzie, W.F., Norton, D.L., and Schmitt, A., 2009, Chemical and thermodynamic model of oil generation in hydrocarbon source rocks: Geochimica Cosmochimica Acta, v. 73, p. 594–695, doi: 10.1016/j.gca.2008.03.004

Hemley, J.J., Montoya, J.W., Marinenko, J.W., and Luce, R.W., 1980, Equilibria in the system Al2 O3 -SiO2 -H2 O and some general implications for alteration/mineralization processes: Economic Geology, v. 75, p. 210– 228.

Holland, H.D., 1959, Some Applications of thermochemical data to problems of ore deposits. stability relations among the oxides, sulfides, sulfates, and carbonates of ore and gangue metals: Economic Geology, v. 54, p. 184-233.

Holland, T., and Powell, R., 2011, An improved and extended internally consistent thermodynamic dataset for phases of petrological interest, involving a new equation of state for solids: Journal Metamorphic Geology, v. 29, p, 333–383.

Halley, S., Dilles, J, and Tosdal, R., 2015, Footprints: Hydrothermal Alteration and Geochemical Dispersion Around Porphyry Copper Deposits: SEG Newsletter, no. 100, p. 1, 12–17.

Holland, H. D., 1959, Some Applications of thermochemical data to problems of ore deposits.stability relations among the oxides, sulfides, sulfates, and carbonates of ore and gangue metals: Economic Geology, v. 54, p. 184-233.

Hughes, Jacob, "Geothermobarometry and Petrographic Interpretations of Christensen Ranch Meta- Banded Iron Formation from the Ruby Range, Montana" (2015). Honors College

James, H.L., 1990, Precambrian geology and bedded iron deposits of the southwestern Ruby Range, Montana: U.S. Geological Survey Professional Paper 1495, 39 pp.

John, D.A., Ayuso, R.A., Barton, M.D., Blakely, R.J., Bodnar, R.J., Dilles, J.H., Gray, F., Graybeal, F.T., Mars, J.C., McPhee, D.K., Seal, R.R., Taylor, R.D., and Vikre, P.G., 2010, Porphyry copper deposit model, ch. B, in Mineral deposit models for resource assessment: U.S. Geological Survey Scientifi c Investigations Report 2010–5070–B, 169 p. 56 Special Publication 123, Montana Mining and Mineral Symposium 2021

Johnson, J., Oelkers, E., and Helgeson, H., 1992, SUPCRT92: A software package for calculating the standard molal thermodynamic properties of minerals, gases, aqueous species, and reactions from 1 to 5000 bar and 0 to 1000°C: Computers and Geoscience, v. 18, no. 7, p. 899–947.

Kats, A., Haven, Y., and Stevels, J., 1962, Hydroxyl groups in alpha quartz: Phys. Chem. Glasses 3, p, 69-75.

Khashgerel, B., Kavalieris, I., and Hayashi, K., 2008, Mineralogy, textures, and whole-rock geochemistry of adanced argillic alteration: Hugo Dummett porphyry Cu–Au deposit, Oyu Tolgoi mineral district, Mongolia: Mineralia Deposita, v. 43, p. 913–932.

Lewis, G., and Randall, 1961, Thermodynamics, revised by Pitzer, K. and Brewer, L, McGraw Hill, p. 173-175.

Lowell, J.D., and Guilbert, J., 1970, Lateral and vertical alteration-mineralization zoning in porphyry ore deposits: Economic Geology, v. 65, p. 373–408.

Luhr, J., 1982, Primary igneous anhydrite: Progress since its recognition in the 1982 El Chichón trachyandesite: Journal of Volcanology and Geothermal Research, v. 175, p. 394–407.

Luhr, J., Carmichael, I., and Varekamp, J., 1984, Journal of Volcanology and Geothermal Research, v. 23, p. 69-108.

Mavrogenes, J. and Bodnar, R., 1994, Hydrogen movement into and out of fluid inclusions in quartz: Experimental evidence and geologic implications: Geochimica et Cosmochimica Acta Volume 58, Issue 1, p. 141-148.

Meyer, C., and Hemley, J.J., 1967, Wall rock alteration, in Barnes, H.L., ed., Geochemistry of hydrothermal ore deposits: N.Y., Holt, Rinehart, and Winston, p. 166–232.

Norton, D., and Knight, J., 1977, Transport Phenomena in Hydrothermal Systems: American Journal of Science, v. 277, p. 937-981.

Parmigiani, A., Degruyter, W., Leclaire, S., Huber, C., and Bachmann, O.,2017, The mechanics of shallow magma reservoir outgassing. Geochemistry, Geophysics, Geosystems, 18(8), p. 2887–2905.

Parmigiani, A., Faroughi, S., Huber, C., Bachmann, O., and Su, Y., 2016, Bubble accumulation and its role in the evolution of magma reservoirs in the upper crust. Nature, 532(7600), p. 492.

Lewis, G, and Randall, M. Revised by Pitzer, K. and Brewer, L., 1961, Thermodynamics, 2nd Edition, McGraw Hill, p. 173.

Richards, J., 2015, The oxidation state, and sulfur and Cu contents of arc magmas: implications for metallogeny: Lithos, v. 233., p. 27-45.

Roberts, S.A., 1973, Pervasive early alteration in the Butte district, Montana, in Miller, R.N., ed., Guidebook for the Butte fi eld meeting of the Society of Economic Geologists: Society of Economic Geologists Guidebook, Anaconda Company, Butte, Montana, p. HH1–HH8.

Roberts, S.A., 1975, Early hydrothermal alteration and mineralization in the Butte district, Montana: Harvard University, Ph.D. dissertation, 157 p. 57 Montana Bureau of Mines and Geology

Rovetta, M., Blacic, J., Hervig, R., and Holloway, J., 1989, An Experimental Study of Hydroxyl in Quartz Using Infrared Spectroscopy and Ion Microprobe Techniques: Journal of Geophysical Research, v. 94, No. B5, p. 5840-5850.

Rumble, D., Duke, E., and Hoering, T., 1986, Hydrothermal graphite in New Hampshire: Evidence of carbon mobility during regional metamorphism: GEOLOGY, v. 14, p. 452-455,

Rutherford, M., 1993, Experimental Petrology Applied to Volcanic Processes: EOS, Transactions, American Geophysical Union, v. 74, no. 5, p. 49-55.

Salotti, C.A., Heinrich, E.W., and Giardini, A.A., 1971, Abiotic carbon and the formation of graphite deposits: Economic Geology, v. 56, p. 929-932.

Sillitoe, R., 2010, Porphyry copper systems: Economic Geology, v. 105, no. 1, p. 3–41.

Strauch, B., Pilz, P., Hierold, J., and Zimmer, M., 2023, Experimental simulations of hydrogen migration through potential storage rocks: International Journal of Hydrogen Energy, v. 48, p. 25808-25820.

Worthington, J.E., 2007, Porphyry and other molybdenum deposits of Idaho and Montana: Idaho Geological Survey Technical Report 07-3, 22 p.

Zimmer, K., Zhang, Y., Peng, L., Yanyan, C., Guanru, Z., Mehmet, D., and Zhu, C., 2016, SUPCRTBL: A revised and extended thermodynamic dataset and software package of SUPCRT92: Computers & Geosciences, v. 90, part A, p. 9.